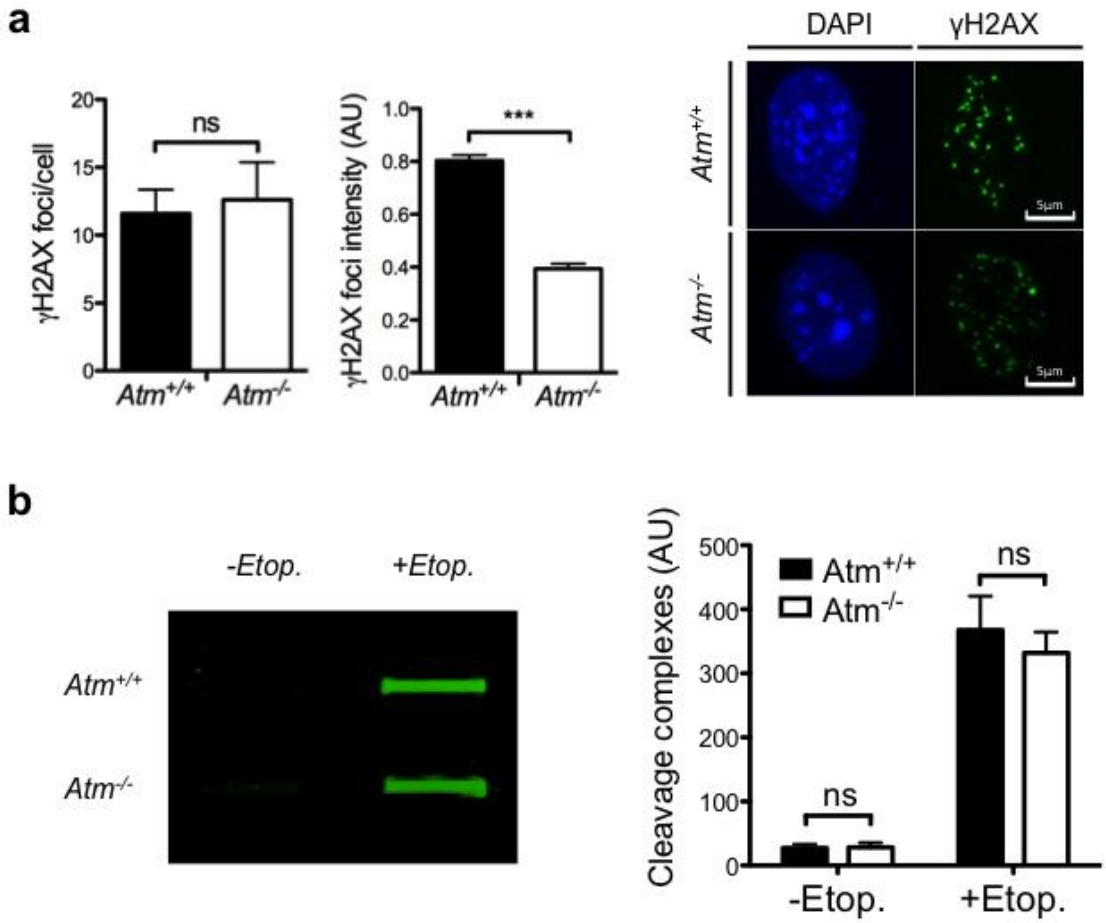

Supplementary Figure 1. ATM does not affect the induction of TOP2-blocked DSBs. (**a**) Average number per cell (left) and intensity (right) of γH2AX foci after 30 min 10 μM etoposide treatment in the indicated confluency arrested primary MEFs from three independent experiments and statistical significance between cells types by Mann-Whitney test is shown (*p<0.05, **p<0.01, ***p<0.001.) A representative image is also shown. Scale bar corresponds 5 μm. (**b**) Slot-immunoblot (left) and quantification (right) of TOP2β cleavage complexes in *Atm*$^{+/+}$ and *Atm*$^{-/-}$ primary MEFs following 1h treatment with 100 μM etoposide or vehicle. Average ± s.e.m. of the slot intensity from three independent experiments and the statistical significance between cell types by Two-way ANOVA test with Bonferroni post-test is shown.

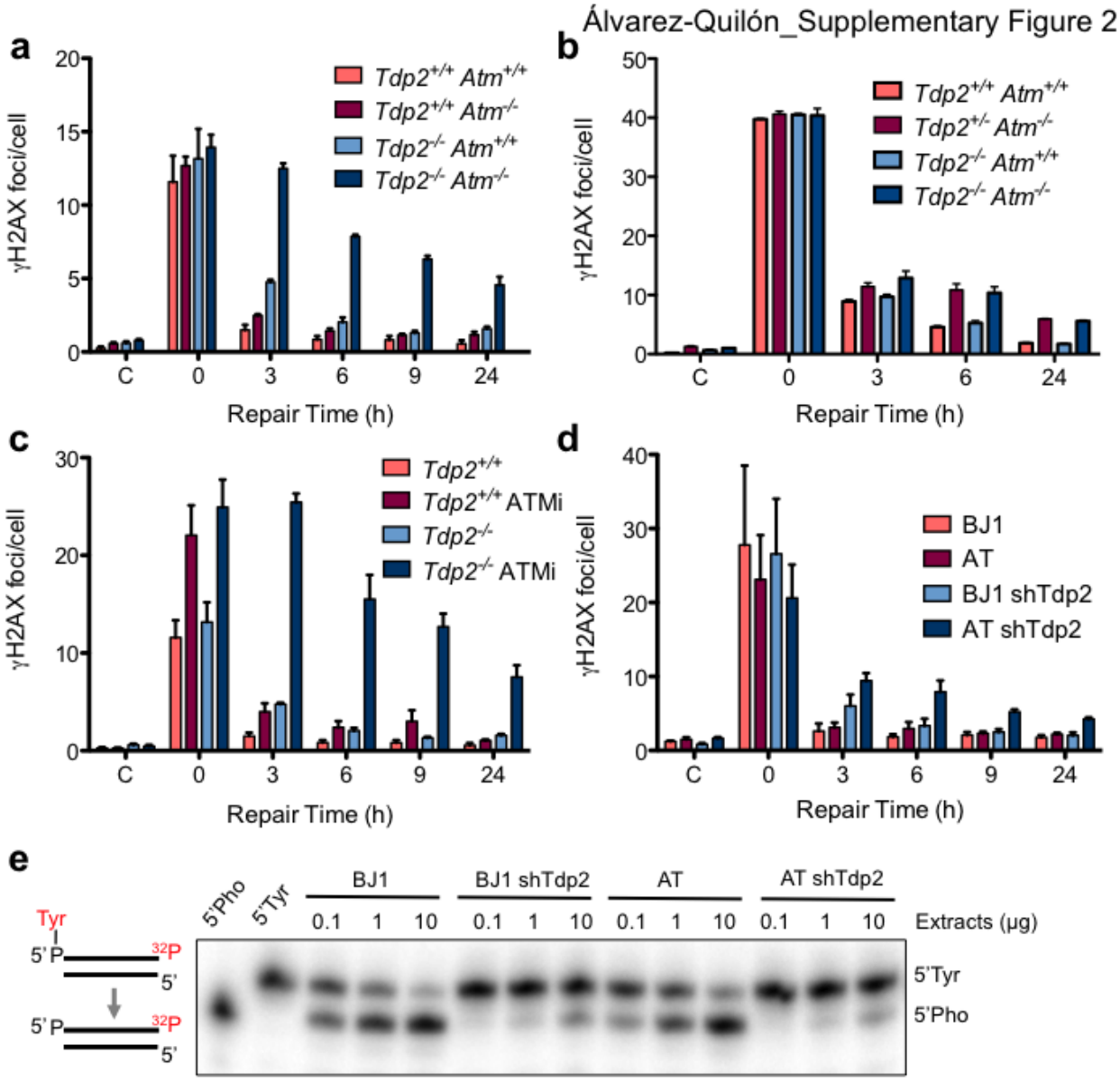

Supplementary Figure 2. ATM facilitates repair of TOP2 blocked DSBs in confluency arrested cells. (**a**) γH2AX foci induction after 30 min 10 μM etoposide treatment and repair at different times following drug removal in the indicated confluency arrested primary MEFs. Average ± s.e.m. of the total number of foci per cell remaining from at least three independent experiments is shown. (**b**) As above, in response to 2 Gy γ-irradiation exposure. 30 min delay is included in each time point to allow foci formation upon induction. (**c**) As above, with or without 10 μM ATM inhibitor incubation. (**d**) As above, in primary fibroblast derived from A-T patients (AT) and wildtype controls (BJ1) depleted (shTDP2) or not for TDP2. In this case, 20 μM etoposide treatment was applied. (**e**) A duplex substrate harbouring a 5' phosphotyrosine blunt end was incubated for 2h with increasing concentration of cellular extracts from primary fibroblast derived from A-T patients (AT) and wildtype controls (BJ1) depleted (shTDP2) or not for TDP2. Migration of the 5'phosphotyrosine (5'Tyr) and 5'phosphate (5'Pho) is indicated. Note that 5' tyrosyl DNA phosphodiesterase activity is still observed in TDP2-depleted cells.

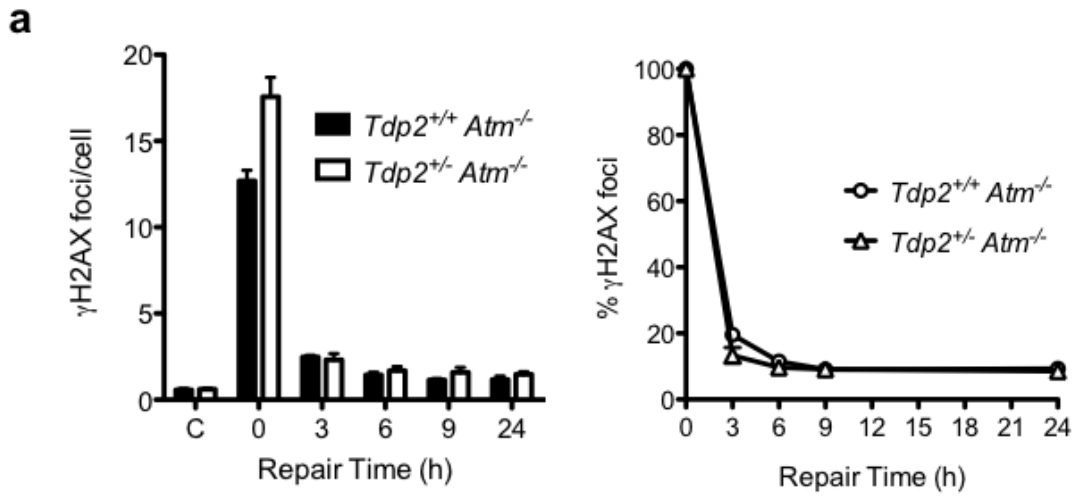

Supplementary Figure 3. Comparison of DSB-repair efficiency between *Tdp2*$^{+/+}$ and *Tdp2*$^{+/-}$ cells in ATM-deficient background. γH2AX foci induction after 30 min 10 μM etoposide treatment and repair at different times following drug removal in confluency arrested primary MEFs (left) and time course of γH2AX foci disappearance (right) in confluency arrested primary MEFs. Average ± s.e.m. of the total number/percentage of foci remaining from three independent experiments is shown.

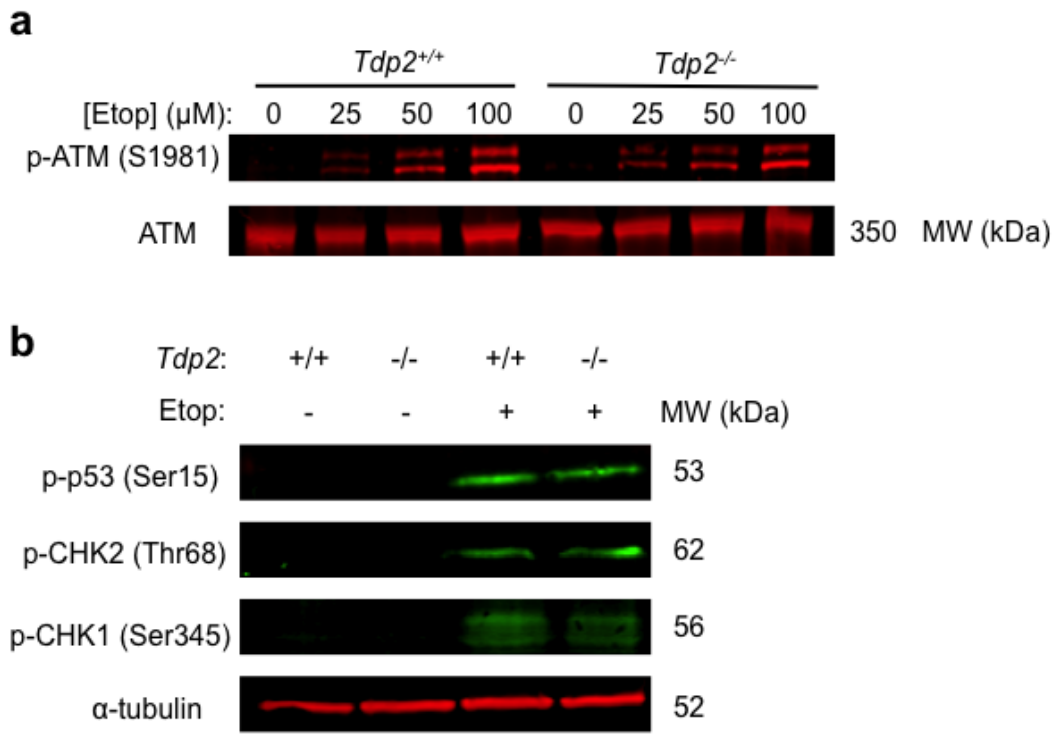

Supplementary Figure 4. Equivalent signalling in response to clean and blocked DSBs. (**a**) ATM activation was monitored by immunoblot of S1981 phosphorylation after 30 min incubation of *Tdp2*$^{+/+}$ and *Tdp2*$^{-/-}$ confluency arrested primary MEFs with the indicated concentrations of etoposide. Total ATM was used as a loading control. (**b**) p53, CHK2 and CHK1 activation was monitored by immunoblot of phosphorylation in the indicated residues after 30 min incubation of *Tdp2*$^{+/+}$ and *Tdp2*$^{-/-}$ confluency arrested primary MEFs with 100μM etoposide. α-Tubulin was used as a loading control.

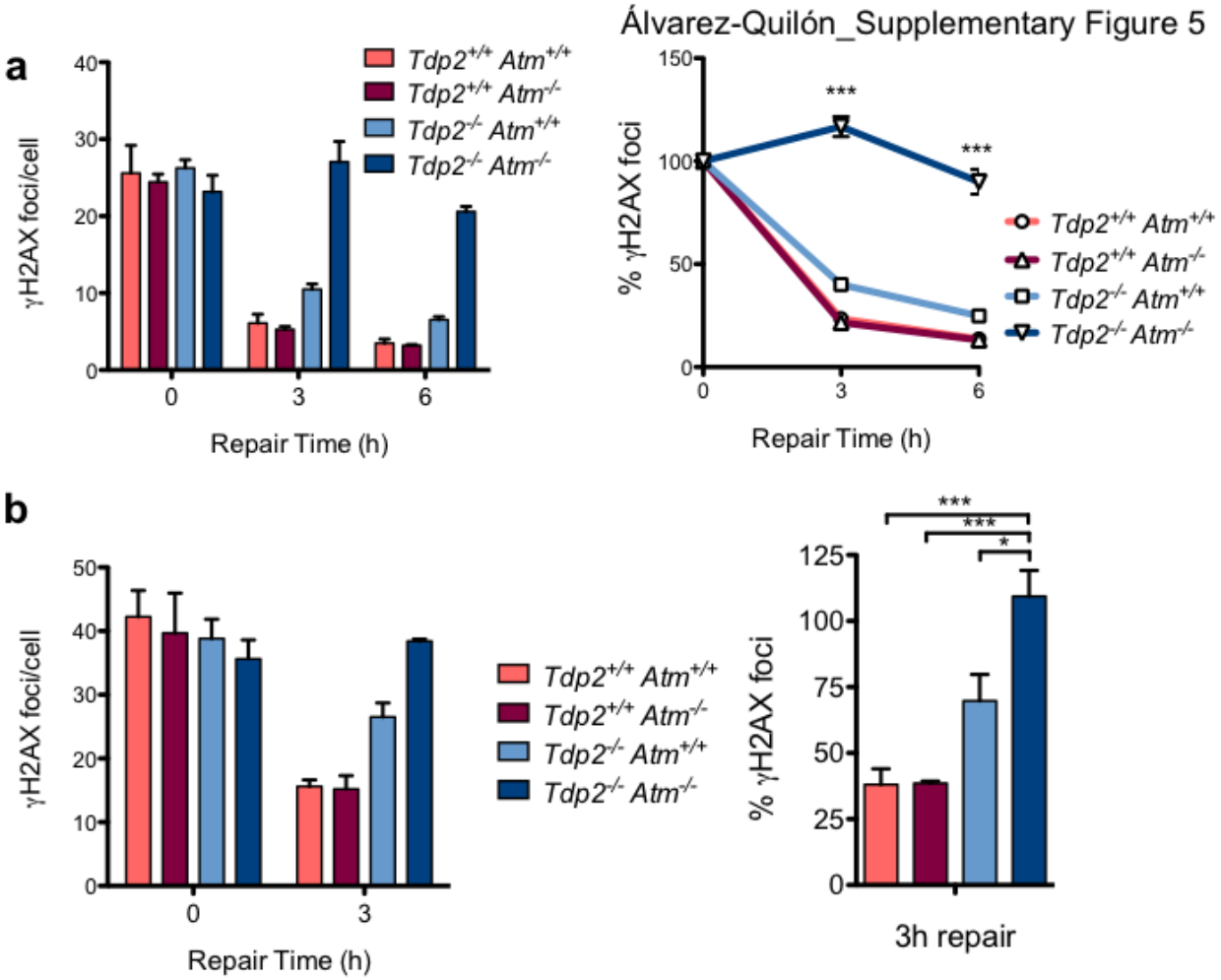

Supplementary Figure 5. ATM facilitates repair of TOP2 blocked DSBs in proliferating cells. (**a**) γH2AX foci induction after 30 min 20 μM etoposide treatment and repair at different times (left) and time course of γH2AX foci disappearance (right) following drug removal in the indicated G1 primary MEFs. (**b**) As above, but in G2 cells treated with 10 μM etoposide. Average ± s.e.m. of the total number/percentage of foci remaining from three independent experiments and the minimal statistical significance between cells deficient in both TDP2 and ATM and all other cells by Two-way ANOVA test with Bonferroni post-test is shown (*p<0.05, **p<0.01, ***p<0.001.)

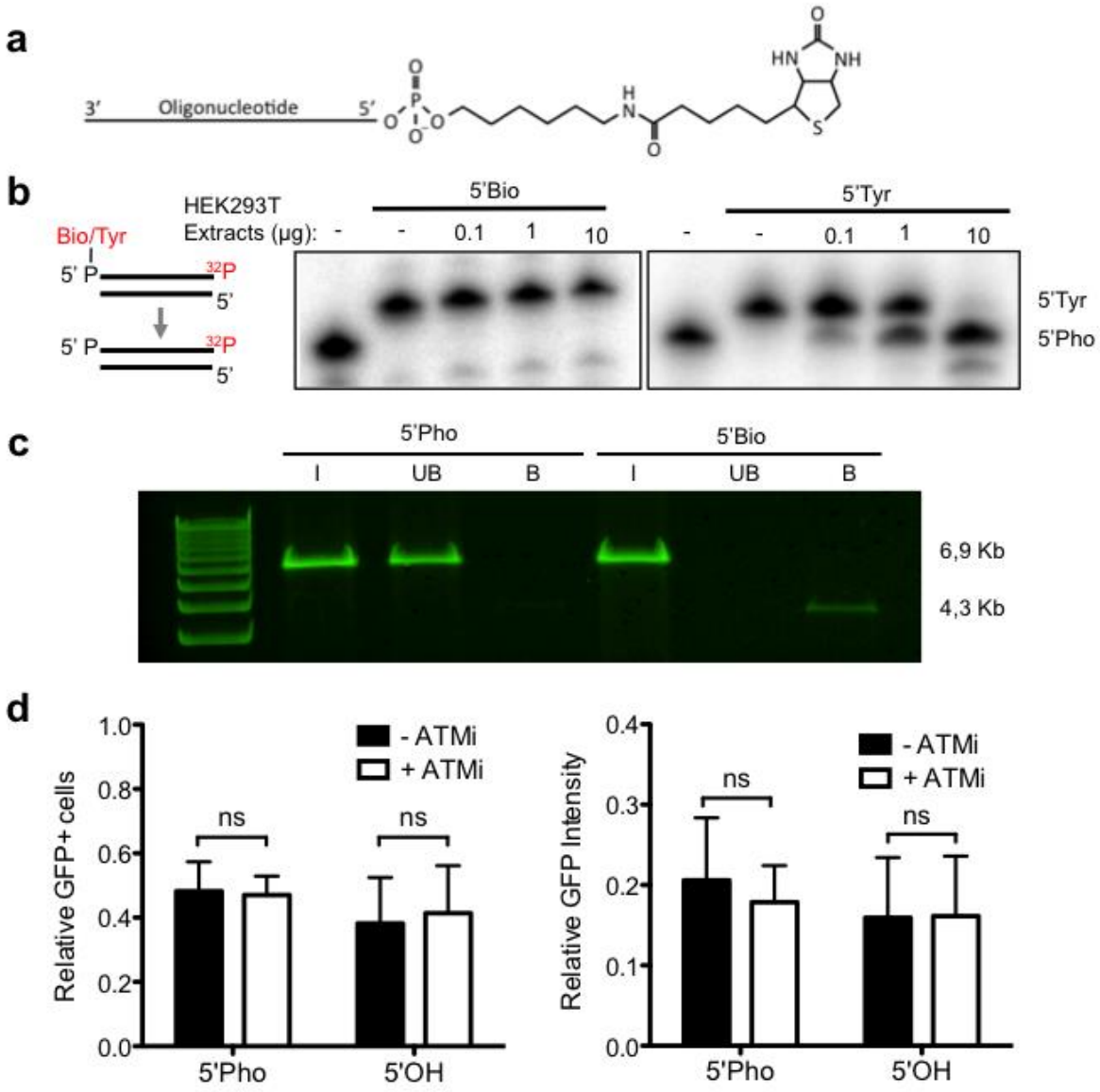

Supplementary Figure 6. (**a**) Scheme of the structure of the 5'-biotin modification used. (**b**) Duplex substrates harbouring a 5'-biotin (5'Bio) or a 5'-tyrosine (5'Tyr) blunt end were incubated with the indicated concentration of HEK293T cellular extracts for 2 h. Migration of the 5'-biotin, 5'-tyrosine and 5'-phosphate (5'Pho) is indicated. (**c**) Validation of substrates used in Figure 3. Each substrate was incubated with streptavidin-coated magnetic particles. Input (I) 5'-phosphate DNA remains unbound (UB), while 5'-biotin is bound (B) as determined by elution with restriction endonucleases. (**d**) HEK293T cells were transfected in the presence or absence of 10 μM ATM inhibitor with the substrates described above, and analysed by FACS for GFP-positive cells (left) and average GFP intensity (right). In both cases, data are relative to transfection with a control pEGFP-Pem1 circular plasmid. Average ± s.e.m. of four independent experiments and statistical significance by Two-way ANOVA with Bonferroni post-test are shown.

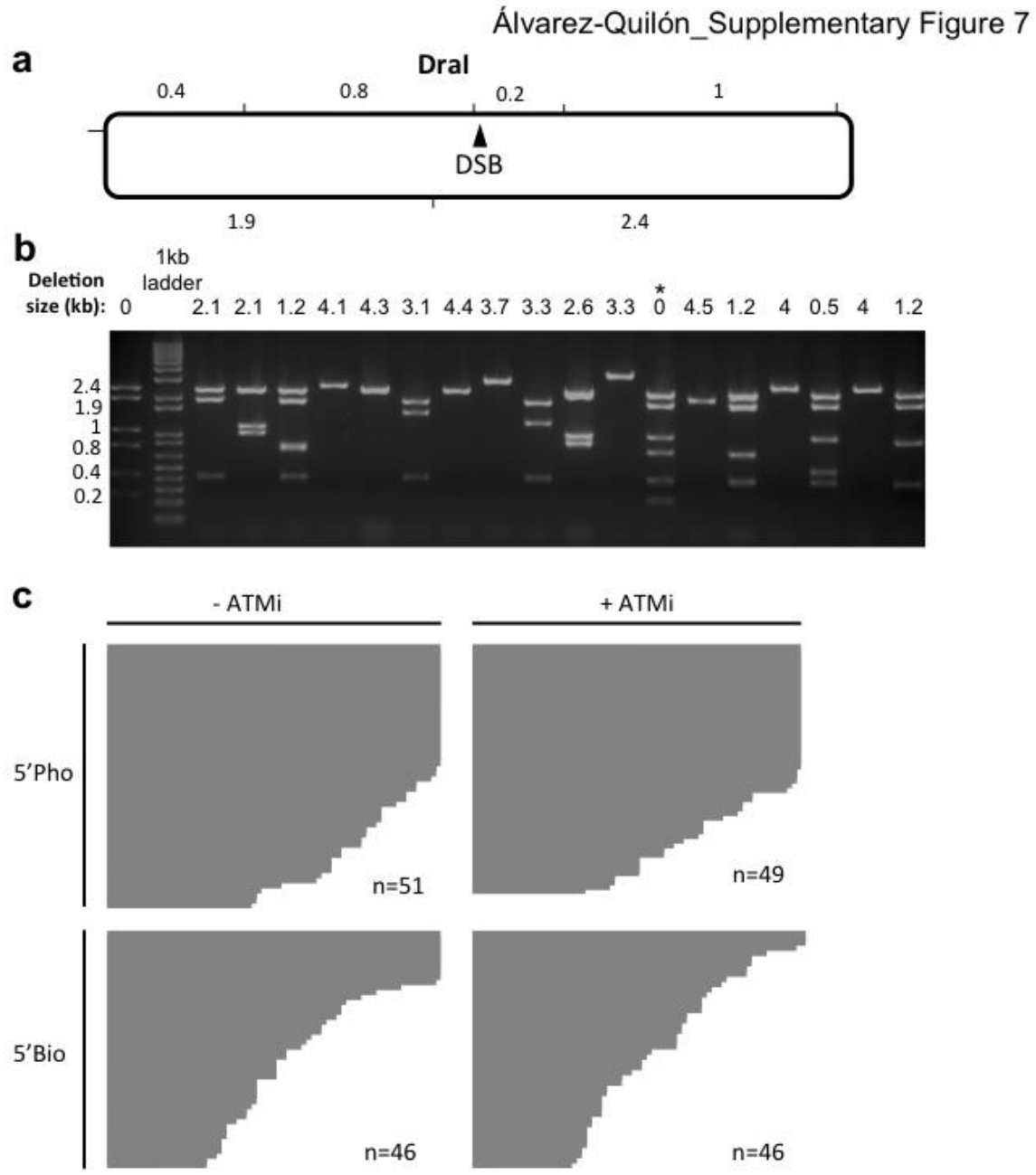

Supplementary Figure 7. (**a**) *DraI* restriction map of re-circularized pEGFP-Pem1 system. The DSB site is indicated (arrow). (**b**) Example of repair events rescued from HEK293T cells treated with ATMi transfected with 5'Biotin-pEGFP-Pem1 analysed by agarose gel electrophoresis after *DraI* endonuclease enzyme digestion. Deletion size calculated for each individual clone is indicated. Control of pEGFP-Pem1 re-circularized plasmid is shown (lane 1). Asterisk indicates a clone without detectable deletion. (**c**) Scheme of the deletion size observed in all repair events obtained from HEK293T cells transfected with modified pEGFP-Pem1 plasmid harbouring 5'phosphate or 5'biotin ends, incubated with or without 10 μM ATM inhibitor.